MATERIALS CHEMISTRY FRONTIERS

RESEARCH ARTICLE

View Article Online
View Journal

Cite this: DOI: 10.1039/d6qm00340k

Customization of cloud temperature in amphiphilic π-systems by photoisomerization and supramolecular co-assembly for smart window applications

Dipak Patra[ab] and Ayyappanpillai Ajayaghosh *[abc]

Controlling the phase transition temperature of amphiphilic polymers and small molecular systems exhibiting the lower critical solution temperature (LCST) phenomenon is crucial to regulate the transmittance of light, required for the construction of thermoresponsive smart windows. To address this problem, we have taken advantage of photoisomerization and supramolecular co-assembly of two photoresponsive amphiphilic molecules, an anthracene-derived cyanostilbene (**ANT**) and a pyrene-derived cyanostilbene (**PYR**), exhibiting different LCST phase transitions at 27 and 37 °C, respectively. Initially, aqueous solutions (1 mM) of these molecules, when heated above their LCST under ambient light, exhibited a 90% reduction in solar light transmittance owing to the increase in particle size from 10–20 nm to 0.6–1.3 μM. Subsequently, the phase transition cloud temperatures (T_{cloud}) could be customized by photoisomerization and co-assembly of the two molecules at different molar ratios. This approach allowed control of the particle size between 675 and 1300 nm during the LCST phase change, enabling the fine-tuning of T_{cloud} between 27 and 37 °C. Smart windows fabricated with **ANT** and **PYR** and their 1 : 1 combination exhibited solar and luminous transmittance reduction from 81% and 84% to 1.7% and 1.6%, respectively, at 27 °C. Thermal IR transmittance was drastically reduced from 78% to 1.8%. This approach has been used to design several custom-made smart window prototypes with controlled transparency modulation suitable for tropical climates.

Received 30th April 2026,
Accepted 25th May 2026

DOI: 10.1039/d6qm00340k

rsc.li/frontiers-materials

Introduction

Lower critical solution temperature (LCST) is an entropy-driven phase change from fibrillar to globular structures exhibited by certain amphiphilic polymers such as polyacrylamide in an aqueous medium.[1–4] These materials undergo phase transitions from transparent to opaque states and *vice versa* in response to external temperature, thus regulating the transmittance of heat-generating IR radiation by facilitating the scattering of solar radiation.[5–8] Hence, they are used for the construction of thermoresponsive smart windows.[9–11] When compared to the photo- and electrochromic smart windows, thermoresponsive polymer-based windows exhibit remarkable advantages, including passive control of sunlight with zero energy input, and are thus relatively cheap and easy to construct and operate.[12–18] However, polymers have several disadvantages, such as inconsistency in molecular weight with batchwise synthesis and the associated variations in particle size formation, which adversely impact the scattering efficiency required for the filtering of the heat generating IR radiations.[19–22]

Nanoarchitectonics represents an emerging paradigm based on chemical and physical material transformation *via* dynamic molecular assembly.[23] The advancement of molecular nanoarchitectonics in materials science results in the creation of stimuli-responsive dynamic materials, opening pathways for a broad spectrum of applications. This concept can be extended for the customization of the operating temperature of smart windows for different climate conditions. One of the major challenges in smart window design is the synthesis of copolymers with the required molecular weight for controlled particle size formation. A possible solution to some of these problems is the use of thermoresponsive amphiphilic small molecules as the phase change material.[24–29] In this context, amphiphilic π-systems are emerging as an alternative to polymers for the construction of thermoresponsive smart windows.[30,31]

When compared to polyacrylamides, the use of LCST-active small molecular π-systems that are capable of forming

[a] *Chemical Sciences and Technology Division, CSIR-National Institute for Interdisciplinary Sciences and Technology (CSIR-NIIST), Thiruvananthapuram 695019, India*
[b] *Academy of Scientific and Innovative Research (AcSIR), Ghaziabad-201002, India*
[c] *SRM Institute of Science and Technology, Kattankulathur, Chennai 603203, India. E-mail: ajayagha@srmist.edu.in*

supramolecular assemblies has the advantage of defined molecular weight, tuneable optical properties and morphological features by synthetic modifications.[32–36] Nevertheless, such approaches have not been widely exploited for designing smart windows with customizable cloud temperature. Another challenge with smart window design is the autonomous control of transparency in response to outdoor light and temperature.[37–40] In order to achieve these objectives, we applied the basic principles of light-induced photoisomerization combined with supramolecular co-assembly of amphiphilic π-systems, leading to significant control over the phase change particle size, thereby regulating light scattering and the associated transparency modulation.[41–46] Although supramolecular chemistry of small molecular π-systems has been at the center stage of advanced materials research for several decades, they are least exploited for the construction of autonomous thermoresponsive smart windows with customizable cloud temperatures.[47–50]

Herein, we present two small molecular amphiphilic π-systems, **ANT** and **PYR**, exhibiting the LCST phenomenon with distinct optical properties and self-assembly behavior as shown in Scheme 1. These monomers and their combinations undergo controlled self-assembly/co-assembly in water below their LCST, resulting in transparent solutions consisting of nonspherical nanoaggregates (10–20 nm) as confirmed by the non-sigmoidal DLS correlogram. However, when heated above the LCST, supramolecular agglomeration of the initially formed nanoaggregates to spherical particles of larger size (0.6–1.3 μM) occurs as established by the sigmoidal correlogram of the DLS spectra, and, as a consequence, the solution became opaque. Exposure of the aqueous solutions of the molecules under UV light lowered the T_{cloud} from 27 to 25 °C in the case of **ANT** and from 37 to 34 °C in the case of **PYR**. The beauty of the present system is the possible fine-tuning of the particle size during the LCST phase change as per the requirement by co-assembling with different ratios of **ANT** and **PYR**, allowing the systematic modulation of T_{cloud} between 27 and 37 °C, a temperature range that is most appropriate for tropical climates. A 10 × 10 cm^2 prototype window can achieve excellent solar light transmittance modulation (79% ΔT_{solar}, 82% ΔT_{lum}, and 76% ΔT_{IR}) with excellent stability for multiple heating and cooling cycles compared with reported systems in the literature.[51–53]

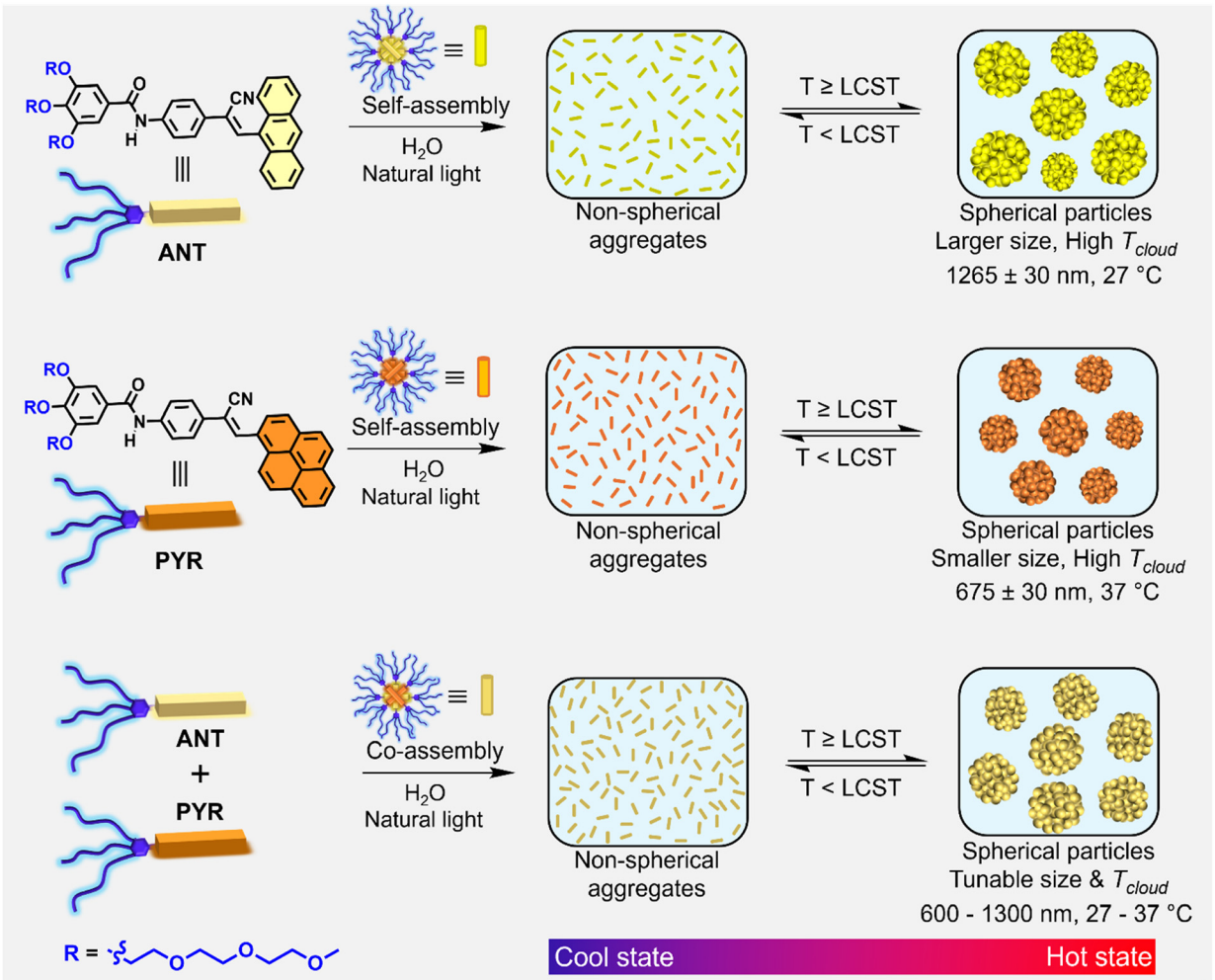

Scheme 1 Schematic illustration of a co-assembly approach for particle size control using two structurally different LCST active amphiphilic π-systems, **ANT** and **PYR**, enabling autonomous transparency modulation. The non-spherical nanoaggregates allow passage of light to appear transparent, whereas the spherical microparticles scatter light to appear opaque.

Results and discussion

We have synthesized two amphiphilic supramolecular π-systems, **ANT** and **PYR**, attached with triethylene glycol monomethyl ether chains on the aromatic core to impart hydrophilicity, aiming at LCST-induced thermoresponsive behavior in water. These molecules were synthesized through the Knoevenagel condensation reaction as per reported procedures (Scheme S1)[31] and characterized by spectral analyses (Fig. S31–S38). Since cyanostilbenes are known to undergo multiple photoreactions such as *Z*/*E*-isomerization, [2+2]-cycloaddition, and Mallory photocyclization, the molecules **ANT** and **PYR** are carefully chosen in such a way that they undergo exclusively *Z*/*E*-photoisomerization owing to the steric bulkiness of the anthracene and pyrene moieties (Fig. 1a).[54–56] The formation of cyclized products was ruled out by the observed reversible change in the time-dependent UV-Vis absorption spectra at elevated temperature (Fig. 1b and c). The UV-Vis absorption spectra of **ANT** and **PYR** were recorded in water ($c = 5 \times 10^{-5}$ M), which exhibited absorption maxima at 254 and 399 nm for **ANT** and at 299 and 395 nm for **PYR**, respectively. UV-Vis, NMR, and FT-IR spectral analyses revealed the formation of molecular assemblies in an aqueous medium through intermolecular hydrogen bonding and π–π stacking (Fig. S1–S4). Upon photoirradiation at 370 nm, both molecules exhibited a gradual decrease in their absorption maxima through an isosbestic point at 304 nm for **ANT** and 299 nm for **PYR**. A photostationary state was achieved within 10 min of irradiation in the case of **ANT**, whereas **PYR** took 80 min to reach the photostationary state, indicating relatively fast isomerization of the former when compared to the latter. At the photostationary state, the *Z*-isomer of **ANT** was converted to 82% of the *E*-isomer as calculated from the UV-Vis absorption spectral change.

Interestingly, in both cases, the thermal back isomerization is found to be sluggish even after keeping the solution in the dark for several days, and the solution needed to be heated above 80 °C to observe the reverse isomerization (Fig. S5–S8 and Tables S1, S2). The isomer ratios for **ANT** were 14 : 86 (*Z* : *E*) at the photostationary state (PSS) when irradiated at 370 nm (370_{PSS}) and 90 : 10 (*Z* : *E*) when heated above 80 °C. For **PYR**,

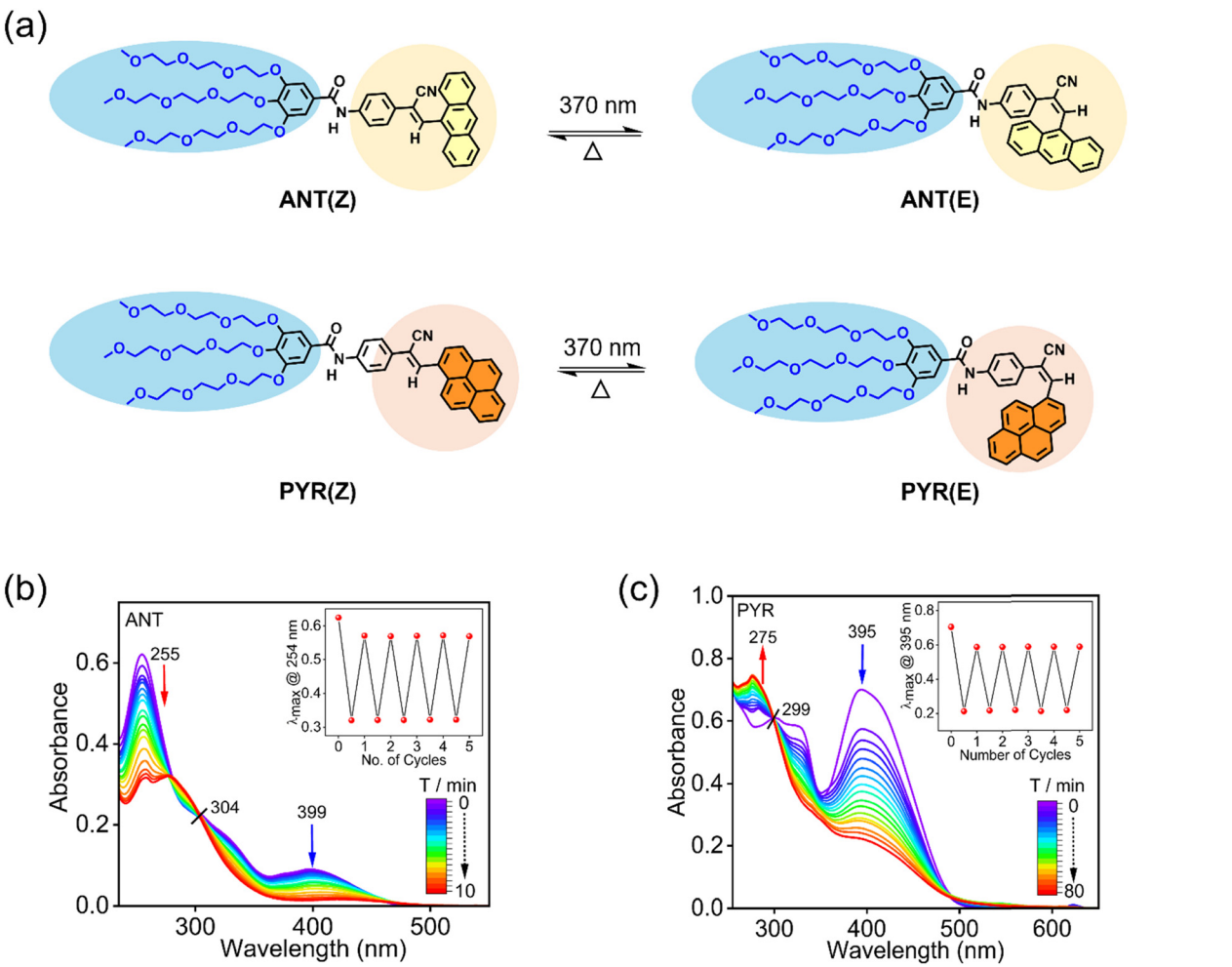

Fig. 1 (a) Structures of **ANT(*Z*)** and **PYR(*Z*)** and their photoisomerization upon irradiation with 370 nm light. (b) and (c) The corresponding changes in the UV-Vis absorption spectra of **ANT(*Z*)** and **PYR(*Z*)** in water ($c = 5 \times 10^{-5}$ M), respectively. Insets show the respective reversible *Z*/*E*-isomerization under photoirradiation and thermal conditions at the photostationary state.

the isomer ratios were 30 : 70 (Z : E) at the PSS (370 nm) and 84 : 16 (Z : E) when heated (above 80 °C). The reversible isomerization plots shown in the insets of Fig. 1b and c indicate that, after the first round of irradiation, a complete thermal recovery of the Z-isomers could not be achieved even after prolonged heating, as seen from the UV-Vis spectral change (Fig. S5 and S6). Both **ANT** and **PYR** exhibited reversible $Z \rightarrow E$ photoisomerization over multiple cycles, without any sign of photodegradation, demonstrating high fatigue resistance. **ANT** and **PYR** underwent Z/E-photoisomerization when illuminated by solar light, albeit less efficiently than under 370 nm light (Fig. S9).

Variable-temperature UV-Vis absorption and ^{1}H NMR spectroscopy revealed the temperature-induced LCST phase transition in water (Fig. S10–S16). The photographs of the reversible phase change of **ANT** solution are shown in Fig. 2a. The transparent solution of **ANT** in water (1 mM) turned opaque when heated to 27 °C or when irradiated at 370 nm, which turned cloudy again upon heating above the LCST. The temperature-induced phase change and the optical color variation are reversible for heating and cooling processes.

When irradiated to reach photostationary states, the respective solutions turned opaque while maintaining the initial solution temperature, indicating a photoinduced lowering of T_{cloud}. The effect of photoirradiation on the LCST phenomenon and the corresponding change in the optical transparency with irradiation time are shown in Fig. 2b and c. The insets in Fig. 2b and c illustrate the corresponding change in T_{cloud} with an increase in the mole fraction of the E-isomer. In the case of **ANT**, the phase change occurred around 27 °C, whereas **PYR** exhibited a phase change at 37 °C, indicating a difference of 10 °C between the two (Fig. S14 and S15). However, in the case of a 1 : 1 mixture of **ANT** and **PYR**, T_{cloud} appeared around 32 °C (Fig. 3c and Fig. S16). The opaque phase is maintained even after keeping the sample for several days in the dark, indicating that the back isomerization to the Z-isomer does not occur and the solution attained equilibrium between the two isomers at the photostationary state. However, when the sample is cooled below its T_{cloud}, it becomes transparent, and further heating above T_{cloud} forces the solution to become cloudy again. To acquire information regarding the LCST phase change occurring in the molecules, dynamic light scattering (DLS) studies were performed below and above transition temperatures (Fig. 3). The corresponding particle size distributions are shown in the insets of Fig. 3. In all cases, DLS data revealed the presence of smaller non-spherical aggregates below the LCST and larger spherical particles above the LCST. DLS data of **ANT** in water (c = 1 mM)

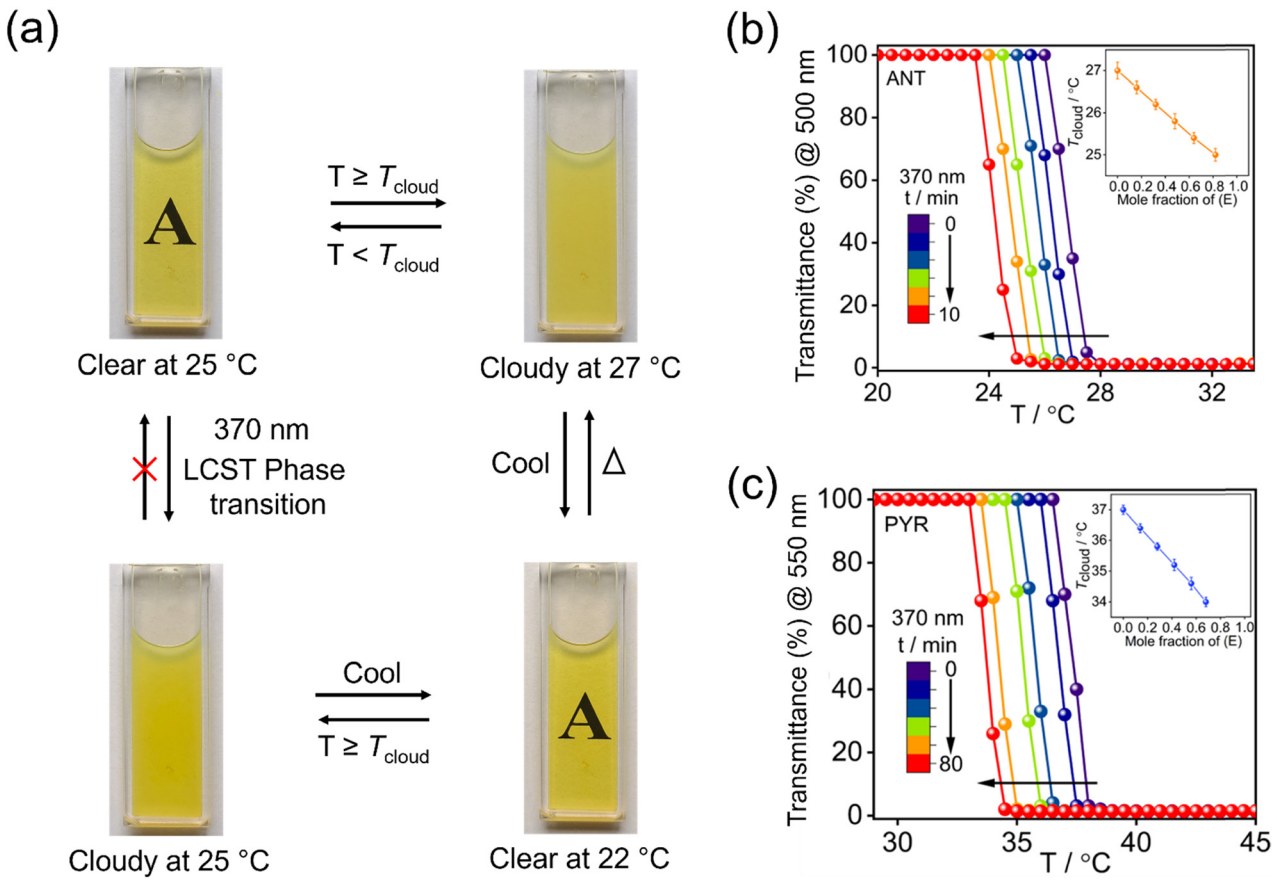

Fig. 2 (a) Photographs corresponding to the LCST phase transition of **ANT** under photochemical and thermal conditions (the letter '**A**' is visible wherever the solution is transparent). (b) and (c) Changes in the light transmittance of **ANT** and **PYR** at different temperatures with continuous irradiation at 370 nm. Insets show the corresponding changes in T_{cloud} with an increase in the mole fraction of the E-isomer.

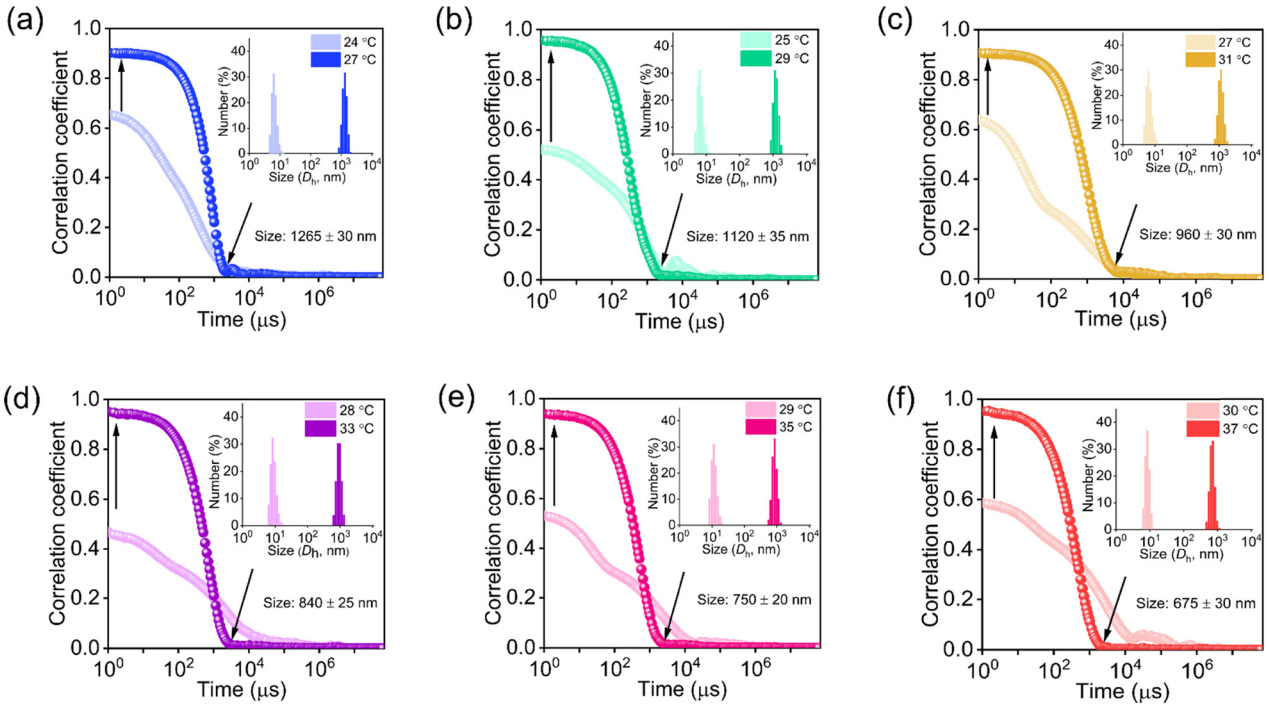

Fig. 3 DLS correlation decay profile with time for the co-assembled states: (a) 1 : 0, (b) 0.8 : 0.2, (c) 0.6 : 0.4, (d) 0.4 : 0.6, (e) 0.2 : 0.8, and (f) 0 : 1, obtained from ratiometric mixing of **ANT** and **PYR**, respectively, below and above cloud point temperatures in water. Insets show DLS plots of the number of particles (%) *versus* size (D_h, nm) below and above T_{cloud}. The gradual decrease in particle size at their LCST is also shown in the respective figures (inset).

before irradiation initially exhibited a particle size of 10–20 nm at 24 °C and 1265–1300 nm at 27 °C (Fig. 3a), whereas **PYR** exhibited a particle size of 10–20 nm at 30 °C (below T_{cloud}) and 675–700 nm at 37 °C (above T_{cloud}) (Fig. 3f). In all cases, above the LCST, the plots of the correlation coefficients *vs.* time exhibited a sigmoidal curve, which were fitted with a mono-exponential decay function, suggesting the formation of larger spherical particles, resulting in strong light-scattering abilities. These observations are in agreement with the light scattering principle, where the correlogram corresponding to the DLS spectrum is a signature of the non-spherical to spherical particle transition during the LCST phase change. LCST parameters, such as concentration-dependent transmittance, T_{cloud}, particle size variations, and thermal hysteresis of **ANT**, **PYR** and **ANT**/**PYR** (1 : 1), are shown in Fig. S14–S16, respectively. In both cases, after photoirradiation, DLS data exhibited a slight increase in particle size above their respective T_{cloud} values, which is in agreement with the observed decrease in their respective T_{cloud} values (Fig. S17).

Customization of the operating temperature and transparency to meet a specific climate condition is a significant challenge in the design of smart windows. Although supramolecular co-assembly of LCST active molecules has been shown to influence their T_{cloud}, this approach has not been tested for the construction of smart windows.[57] We have successfully implemented this strategy to modulate the T_{cloud} of **ANT** and **PYR** in response to the ambient weather conditions for designing thermoresponsive smart windows. For this purpose, co-assemblies of **ANT** and **PYR** were prepared in different molar ratios in water at around 20 °C. It is found that the T_{cloud} values of the co-assembly systematically vary between the T_{cloud} values of **ANT** and **PYR** upon changing their molar ratios (Fig. 4a). T_{cloud} is found to decrease with an increase in **ANT** content in the co-assembly, as seen from the plot of the transition temperature against the molar ratios (Fig. 4b). Interestingly, the DLS analysis of the co-assembly at different **ANT**/**PYR** compositions revealed the formation of spherical particles above their T_{cloud} values with a significant increase in the hydrodynamic radius as the mole fraction of **ANT** is increased (Fig. 3 and 4c). A dynamic change in the particle size between 675 and 1300 nm at different compositions could be observed, where the particles collapsed at a lower temperature and reformed at a higher temperature (Fig. 4d). The thermal hysteresis of co-assembled **ANT**/**PYR** at different mixing ratios was found to be almost identical (Fig. S18). The LCST phenomenon and the phase change arise from the interplay between the hydrophilic–hydrophobic balance and the intrinsic dipole moments of *Z*/*E*-isomers.[58,59] According to DFT analysis, the *Z*-isomer displays a markedly increased dipole moment relative to the *E*-isomer in both **ANT** and **PYR** derivatives (Fig. S19–S22 and Table S3). Consequently, the T_{cloud} of the *Z*-isomer is higher than that of the *E*-isomer. After evaluating the LCST phenomenon in **ANT**, **PYR** and their combination (1 : 1 molar ratio), we fabricated 10 × 10 cm^2 smart window prototypes using 1 mM aqueous solutions (Fig. 5). The window fabricated with **ANT** exhibited transparent-to-opaque switching at 28 °C with a light greenish yellow color tone and remained opaque with a further increase in temperature (Fig. 5a and Movie S1). However, the window

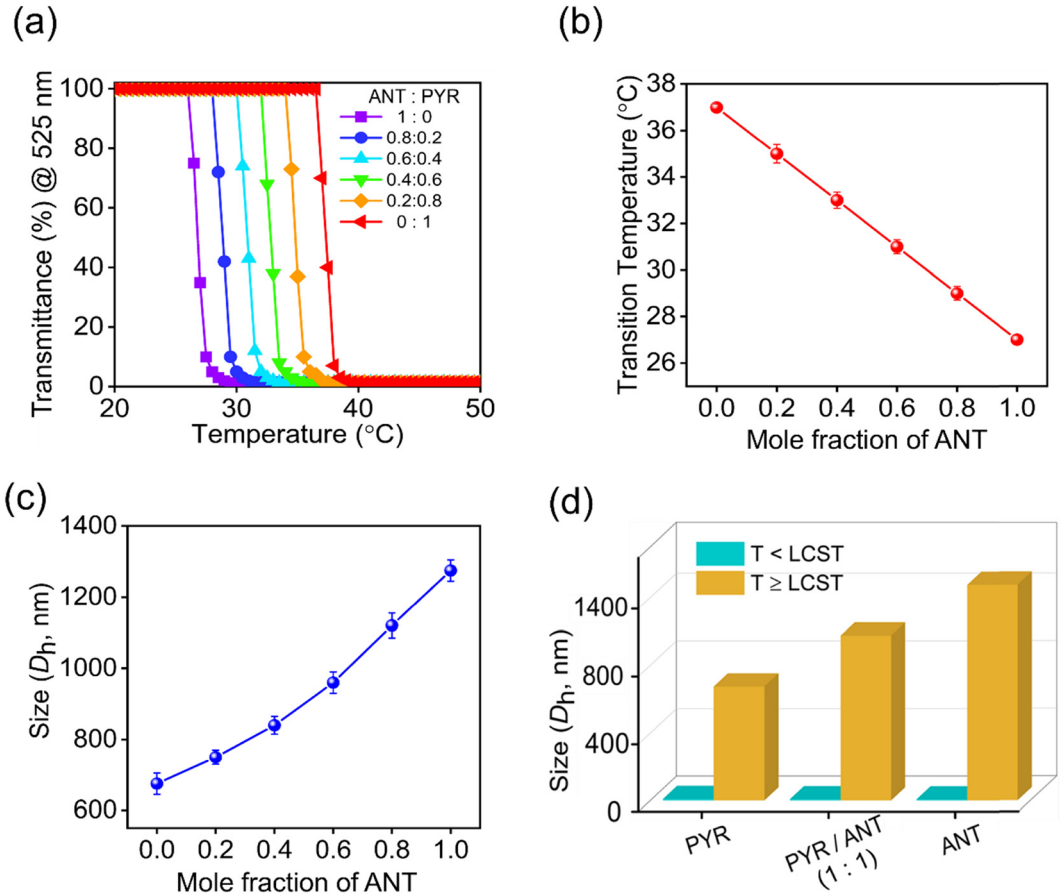

Fig. 4 Plots of LCST parameters at various compositions of **ANT** and **PYR**. (a) %Transmittance *vs.* temperature, (b) T_{cloud} *vs.* **ANT**/**PYR** ratio, (c) hydrodynamic diameter *vs.* **ANT**/**PYR** ratio and (d) the variation of hydrodynamic diameter at different **ANT**/**PYR** ratios, below and above the LCST.

fabricated with **PYR** remained transparent up to 32 °C and turned opaque at 38 °C, showing a 10 °C difference in cloud point temperature (Fig. 5c and Movie S2). In this case, the color tone of the window appeared golden yellow. On the other hand, the window fabricated with a 1 : 1 molar ratio of **ANT** and **PYR** turned opaque at 32 °C with a color tone of light yellow (Fig. 5b and Movie S3). The CIE chromaticity diagram, along with the window's color coordinates below and above the LCST, is shown in Fig. S23. The stability of the windows was tested initially for a 24 h time period between their cloud temperatures by plotting the transmittance spectra *vs.* time (Fig. S24) and then the process was repeated for multiple cycles of operation. The corresponding plots are shown on the side of the respective window in Fig. 5. These plots reveal the high thermal stability of the windows over a wide range of tropical temperatures. The variable-temperature transmittance spectra of **ANT** displayed notably rapid switching times, with a fast response of 10 ± 1 s for the transition from a transparent to an opaque state during heating, and the cooling cycles recorded within 21 ± 2 s (Fig. S25a). In comparison, **PYR** exhibited slightly slower switching characteristics, with heating and cooling cycles recorded within 13 ± 2 s and 30 ± 4 s, respectively (Fig. S25b). The optical transmittance spectra of the **ANT** window, below and above the cloud temperature, in comparison to the solar transmittance spectrum are shown in Fig. 6a. The optical transparency of the window showed 84% transmittance in the visible region (400–780 nm) at 20 °C and 1.7% transmittance at 27 °C. Upon increasing the temperature to 27 °C, the window turned opaque with a greenish-yellow color tone, and the transmittance of solar light approached zero in the UV-Vis-NIR (400–2500 nm) region (Fig. 6a). Notably, the **ANT** windows exhibited higher solar transmittance (T_{solar}) and luminous transmittance (T_{lum}) at low temperatures in comparison with **PYR** windows, whereas the thermal IR transmittance (T_{IR}) remained almost the same in both cases (Fig. 6b and Fig. S26). The stability and consistency of the window in transmitting solar light were further established by plotting T_{solar} and transmittance modulation (%ΔT) for 1000 switching cycles below and above T_{cloud} (Fig. 6c and d). More importantly, even after 10 000 cycles of operation, the transmittance remained almost constant at temperatures below and above the cloud point temperature (Fig. 6e and Fig. S27). Variable-temperature DLS data revealed that the hydrodynamic diameters of **ANT**, **PYR**, and **ANT**:**PYR** (1:1) particles remained unchanged even after multiple heating and cooling cycles, indicating their excellent long-term stability in water (Fig. S28). The combined transmittance performance in both transparent and opaque states under indoor temperature regulation makes **ANT**, **PYR**, and their co-assembled state

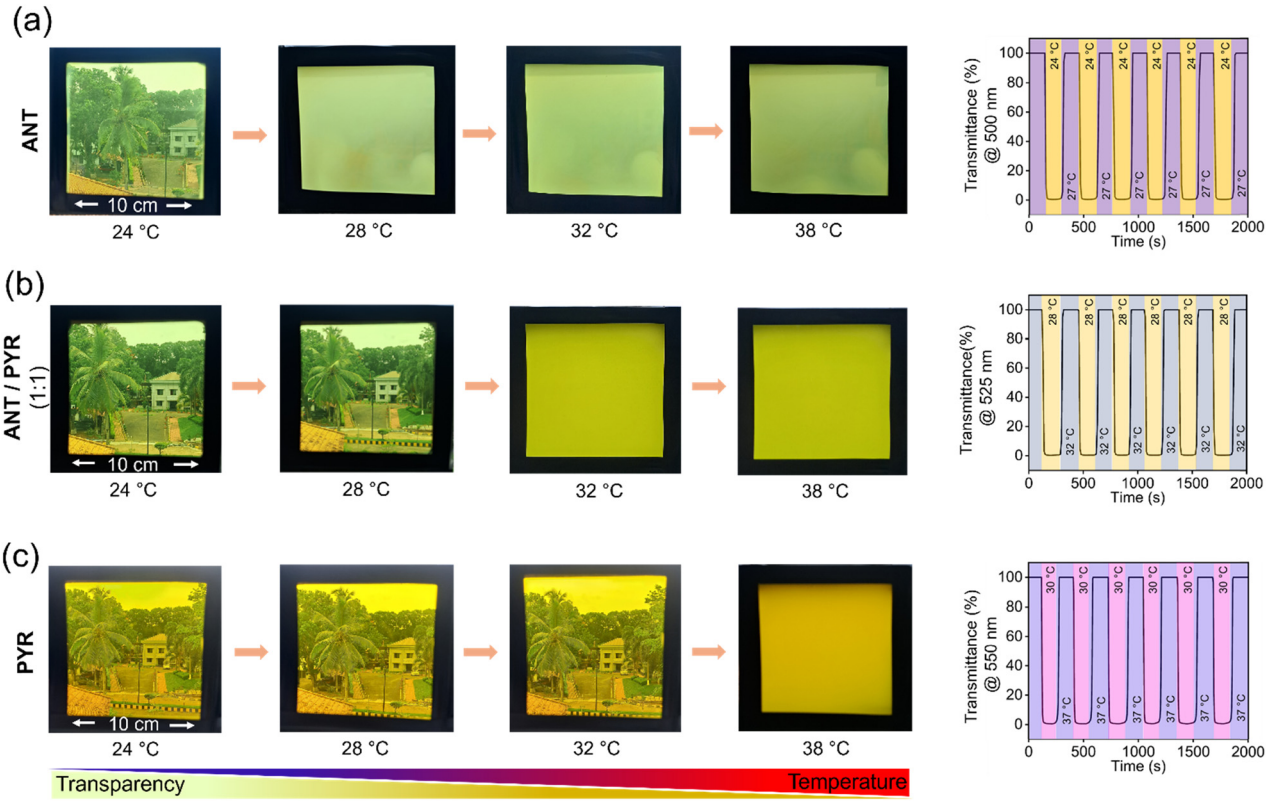

Fig. 5 Solar light-induced transparency modulation of 10 × 10 cm^2 smart window prototypes between 24 and 38 °C and their respective transparency switching operations below and above T_{cloud}. (a) **ANT**, (b) **ANT**/**PYR** (1 : 1), and (c) **PYR**. The outdoor solar light intensity was 1 × 10^3 W m^{-2}.

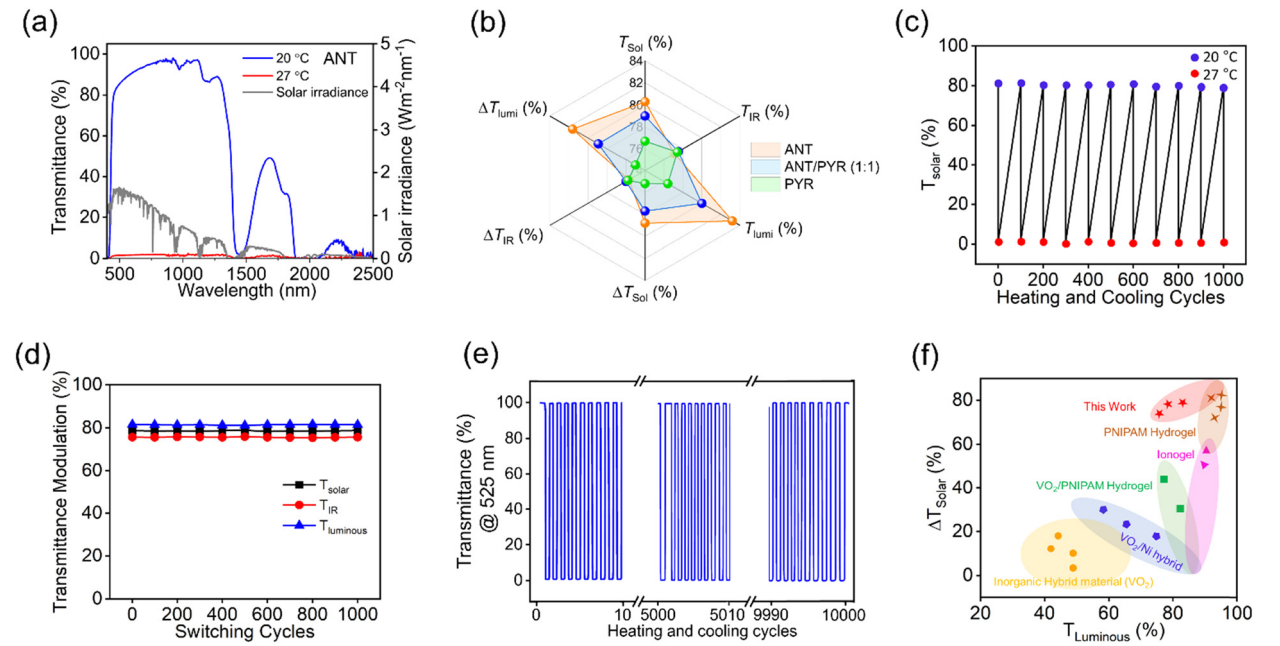

Fig. 6 Solar radiation control performance of a 10 × 10 cm^2 smart window prototype fabricated with **ANT**. (a) Light transmittance spectra above and below the LCST in comparison with the solar radiation spectrum. (b) Solar light scattering pattern of **ANT** in comparison with **PYR** and **ANT**/**PYR** (1 : 1). (c) and (d) Reversible solar transmittance and stable transmittance modulation for 1000 switching cycles. (e) Shelf-life of the **ANT**/**PYR** (1 : 1) window after 10 000 cycles below and above T_{cloud}. (f) Thermochromic performance of the smart window prototypes in this study compared with reported systems in the literature.

promising candidates for smart window applications, offering advantages over conventional thermochromic inorganic, organic, and polymer materials (Fig. 6f). Finally, from the application viewpoint, we fabricated a library of smart window prototypes by a mix-and-match approach, which is usually applied for screening a large number of molecules and materials for specific applications. Four different types of smart window panels using **ANT**, **ANT**/**PYR** (1 : 1), **PYR**, and their combination, namely **A**, **B**, **C**, and **D**, respectively, were fabricated and their performance was evaluated over a temperature range of 24–38 °C (Fig. S29). All modules in window **A** are fabricated with **ANT**, modules in **B** with **ANT**/**PYR** (1 : 1) and modules in **C** with **PYR**, whereas all modules in window **D** are made up of a combination of **ANT**, **ANT**/**PYR** (1 : 1), and **PYR**. It can be seen that all modules in window **A** are transparent at 24 °C and turn opaque at 28 °C and above. When the window panels were fabricated with modules having a 1 : 1 mixture of **ANT**/**PYR** as in **B**, they exhibited a thermal response at 32 °C and above. All modules in window '**C**' are transparent up to 35 °C and turn opaque at 38 °C. It is possible to prepare a number of window modules that respond systematically to temperatures between 24 and 38 °C using different supramolecular combinations of **ANT**/**PYR**, thus providing opportunities for constructing a combinatorial library of smart windows that can autonomously change the transparency and color tone. In addition, window panels having different modules of **ANT**, **PYR** and **ANT**/**PYR** combinations can be constructed as shown in panel '**D**'. The thermal response of panel '**D**' at different temperatures is shown. At 24 °C, all modules are transparent, allowing maximum transparency. When the temperature is increased to 28 °C, the **ANT** module becomes opaque, thereby reducing light transmittance by one-third. Upon further increasing the temperature to 32 °C, the **PYR** module will remain transparent, and the other two become opaque, thus reducing the light transmittance to two-thirds. At 38 °C, all modules become opaque with maximum light blocking. Thus, windows constructed using panel **D** can autonomously control the transparency and color tone with the dynamic variations in atmospheric temperature, which in turn can regulate light and temperature in an indoor space. Furthermore, window panels **A**, **B**, **C**, and **D** provide multiple options to construct a variety of combinatorial modules by changing the percentage of **ANT** and **PYR** in a supramolecular co-assembly mixture. In this way, '16' combinatorial window modules in four types of arrangements with **A**, **B**, **C**, and **D** can be constructed using a mix-and-match approach.

Further mix-and-match can create '64' other combinations as shown in Fig. S30. In principle, with the imagination and creativity of a user, any number of window combinations becomes possible for the construction of large area glass window facades. These window facades are aesthetically appealing and can autonomously modulate their cloud temperature and the light intensity in a closed space in response to changes in external temperature. Integration of such windows into building architecture results in significant energy saving by reducing the energy required for air conditioning, in addition to their aesthetic appeal. The technology development studies for potential commercial applications of the described smart windows are in progress.

Conclusions

The amphiphilic π-systems **ANT** and **PYR** reported here exhibit the LCST phenomenon with phase transition cloud temperatures of 27 and 37 °C, respectively. The cloud point temperature of these molecules can be controlled by photoisomerization and supramolecular co-assembly. Since there is a 10 °C difference in the T_{cloud} of **ANT** and **PYR**, supramolecular co-assembly of these molecules at different molar ratios allows regulation of the solar radiation transmittance over a range of 27–37 °C. The supramolecular phase change and the associated particle size variation above T_{cloud} are crucial in controlling light scattering, thereby autonomously controlling the light transmittance. Prototype (10 × 10 cm^2) windows fabricated with **ANT**, **PYR**, and **ANT**/**PYR** (1 : 1 ratio) exhibited significant changes in solar (81–1.7%), luminous (84–1.6%), and thermal IR transmittance (78–1.8%) during the transparent-to-opaque phase transition at their respective cloud temperatures. Tuning of the cloud temperature by the supramolecular co-assembly approach described here allows the construction of a large number of custom-made smart windows suitable for tropical climates. In conclusion, the described LCST-active supramolecular π-systems can be effectively used as excellent thermoresponsive functional materials for the construction of smart windows that are self-adaptive to the atmospheric temperature and solar radiation.

Author contributions

D. P. performed the synthesis and characterization of the target molecules and the experiments. D. P. and A. G. designed the experiments, discussed the results, analyzed the data, and co-wrote the manuscript. A. G. was responsible for the overall project concept, direction, coordination and project funding.

Conflicts of interest

There are no conflicts of interest to declare.

Data availability

The data supporting this article have been included as part of the supplementary information (SI). Supplementary information is available. See DOI: **https://doi.org/10.1039/d6qm00340k**.

Acknowledgements

D. P. is thankful to the CSIR for a research fellowship and A. A. is grateful to the CSIR for a Bhatnagar Fellowship grant (CSIRHRD/BFS 2024/03/03).

Notes and references

1 J. D. Kocher, A. Mahfouz, J. G. McDaniel and A. K. Menon, Thermodynamic properties of lower critical solution temperature (LCST) mixtures for application in energy–water systems, *Phys. Chem. Chem. Phys.*, 2025, **27**, 15024.

2 A. Agarwal, B. G. Bobay and M. L. Becker, Observation of Dynamic Aggregation Behavior in Thermoresponsive Micro- and Nanoparticles via Diffusion-Ordered NMR Spectroscopy, *J. Am. Chem. Soc.*, 2025, **147**, 9386–9395.
3 S. S. Chittari, A. C. Obermeyer and A. S. Knight, Investigating Fundamental Principles of Nonequilibrium Assembly Using Temperature-Sensitive Copolymers, *J. Am. Chem. Soc.*, 2023, **145**, 6554–6561.
4 V. R. de la Rosa, P. Woisel and R. Hoogenboom, Supramolecular control over thermoresponsive polymers, *Mater. Today*, 2016, **19**, 44–55.
5 K. Ryu, G. Li, K. Zhang, J. Guan, Y. Long and Z. Dong, Thermoresponsive Hydrogels for the Construction of Smart Windows, Sensors, and Actuators, *Acc. Mater. Res.*, 2025, **6**, 379–392.
6 D. Patra, R. D. Mukhopadhyay and A. Ajayaghosh, Lower Critical Solution Temperature Active Supramolecular π-Systems for Smart Applications, *Angew. Chem., Int. Ed.*, 2025, **137**, e202517868.
7 J. Korpanty, L. R. Parent, N. Hampu, S. Weigand and N. C. Gianneschi, Thermoresponsive polymer assemblies via variable temperature liquid-phase transmission electron microscopy and small angle X-ray scattering, *Nat. Commun.*, 2021, **12**, 6568.
8 S. Wu, Q. Zhang, Y. Deng, X. Li, Z. Luo, B. Zheng and S. Dong, Assembly Pattern of Supramolecular Hydrogel Induced by Lower Critical Solution Temperature Behavior of Low-Molecular-Weight Gelator, *J. Am. Chem. Soc.*, 2020, **142**, 448–455.
9 W. Chen, Z. Lin and S. Hu, An All-Weather Sol–Gel Thermochromic Energy-Saving Smart Window, *ACS Appl. Mater. Interfaces*, 2024, **16**, 70863–70873.
10 G. Chen, K. Wang, J. Yang, J. Huang, Z. Chen, J. Zheng, J. Wang, H. Yang, S. Li, Y. Miao, W. Wang, N. Zhu, X. Jiang, Y. Chen and J. Fu, Printable Thermochromic Hydrogel-Based Smart Window for All-Weather Building Temperature Regulation in Diverse Climates, *Adv. Mater.*, 2023, **35**, 2211716.
11 X. H. Li, C. Liu, S. P. Feng and N. X. Fang, Broadband Light Management with Thermochromic Hydrogel Microparticles for Smart Windows, *Joule*, 2019, **3**, 290–302.
12 Z. Du, S. Wang, C. Gu and G. Yang, Recent advances in photo- or electro-chromic smart windows and their thermal regulation, *Responsive Mater.*, 2025, **3**, e20250007.
13 M. J. Moran, M. Magrini, D. M. Walba and I. Aprahamian, Driving a Liquid Crystal Phase Transition Using a Photochromic Hydrazone, *J. Am. Chem. Soc.*, 2018, **140**, 13623–13627.
14 H. Khandelwal, A. P. H. J. Schenning and M. G. Debije, Infrared Regulating Smart Window Based on Organic Materials, *Adv. Energy Mater.*, 2017, **7**, 1602209.
15 Z. Zhang, L. Zhang, Y. Zhou, Y. Cui, Z. Chen, Y. Liu, J. Li, Y. Long and Y. Gao, Thermochromic Energy Efficient Windows: Fundamentals, Recent Advances, and Perspectives, *Chem. Rev.*, 2023, **123**, 7025–7080.
16 A. Nirmala, I. Mukkatt, S. Shankar and A. Ajayaghosh, Thermochromic Color Switching to Temperature Controlled Volatile Memory and Counter Operations with Metal–Organic Complexes and Hybrid Gels, *Angew. Chem., Int. Ed.*, 2021, **60**, 455–465.
17 L. Gonzalez, C. Liu, B. Dietrich, H. Su, S. Sproules, H. Cui, D. Honecker, D. J. Adams and E. R. Draper, Transparent-to-dark photo- and electrochromic gels, *Commun. Chem.*, 2018, **1**, 77.
18 S. Wang, Z. Xu, T. Wang, T. Xiao, X.-Y. Hu, Y.-Z. Shen and L. Wang, Warm/cool-tone switchable thermochromic material for smart windows by orthogonally integrating properties of pillar[6]arene and ferrocene, *Nat. Commun.*, 2018, **9**, 1737.
19 J. Li, P. Gu, H. Pan, Z. Qiao, J. Wang, Y. Cao, W. Wang and Y. Yang, A Facile yet Versatile Strategy to Construct Liquid Hybrid Energy-Saving Windows for Strong Solar Modulation, *Adv. Sci.*, 2023, **10**, 2206044.
20 K. Zhang, M. Zhang, X. Feng, M. A. Hempenius and G. J. Vancso, Switching Light Transmittance by Responsive Organometallic Poly(ionic liquid)s: Control by Cross Talk of Thermal and Redox Stimuli, *Adv. Funct. Mater.*, 2017, **27**, 1702784.
21 G. Xu, H. Xia, P. Chen, W. She, H. Zhang, J. Ma and Q. Ruan, Thermochromic Hydrogels with Dynamic Solar Modulation and Regulatable Critical Response Temperature for Energy-Saving Smart Windows, *Adv. Funct. Mater.*, 2021, **32**, 2109597.
22 Q. Zhang, Y. Jiang, L. Chen, W. Chen, J. Li, Y. Cai, C. Ma, W. Xu, Y. Lu, X. Jia and Z. Bao, Ultra-Compliant and Tough Thermochromic Polymer for Self-Regulated Smart Windows, *Adv. Funct. Mater.*, 2021, **31**, 2100686.
23 K. Ariga, Nanoarchitectonics: the method for everything in materials science, *Bull. Chem. Soc. Jpn.*, 2024, **97**, uoad001.
24 F. D. Jochum and P. Theato, Temperature- and light-responsive smart polymer materials, *Chem. Soc. Rev.*, 2013, **42**, 7468–7483.
25 X. Chi, G. Yu, L. Shao, J. Chen, F. Huang and A. Dual-Thermoresponsive Gemini-Type Supra-amphiphilic, Macromolecular [3]Pseudorotaxane Based on Pillar[10]arene/Paraquat Cooperative Complexation, *J. Am. Chem. Soc.*, 2016, **138**, 3168–3174.
26 T. Yuan, M. Vazquez, A. N. Goldner, Y. Xu, R. Contrucci, M. A. Firestone, M. A. Olson and L. Fang, Versatile Thermochromic Supramolecular Materials Based on Competing Charge Transfer Interactions, *Adv. Funct. Mater.*, 2016, **26**, 8604–8612.
27 P. Wei, T. R. Cook, X. Yan, F. Huang, P. J. Stang and A. Discrete, Amphiphilic Organoplatinum(II) Metallacycle with Tunable Lower Critical Solution Temperature Behavior, *J. Am. Chem. Soc.*, 2014, **136**, 15497–15500.
28 Y. Yang, A. J. Mijalis, H. Fu, C. Agosto, K. J. Tan, J. D. Batteas and D. E. Bergbreiter, Reversible Changes in Solution pH Resulting from Changes in Thermoresponsive Polymer Solubility, *J. Am. Chem. Soc.*, 2012, **134**, 7378–7383.
29 K. Belal, F. Stoffelbach, J. Lyskawa, M. Fumagalli, D. Hourdet, A. Marcellan, L. De Smet, V. R. de la Rosa, G. Cooke, R. Hoogenboom and P. Woisel, Recognition-

Mediated Hydrogel Swelling Controlled by Interaction with a Negative Thermoresponsive LCST Polymer, *Angew. Chem., Int. Ed.*, 2016, **128**, 14180–14184.

30 S. Das, D. Patra, S. Shankar and A. Ajayaghosh, Photocycloaddition as a Tool for Modulation of the Lower Critical Solution Temperature in a Molecular π-System to Control Transmission of Solar Radiation, *Angew. Chem., Int. Ed.*, 2022, **61**, e202207641.

31 D. Patra, S. Das, S. Shankar and A. Ajayaghosh, The Nanoarchitectonics of Sustainable Smart Window Design by LCST Modulation of Photoresponsive Molecular π-Systems, *Adv. Funct. Mater.*, 2024, **34**, 2408014.

32 H.-Q. Peng, B. Liu, P. Wei, P. Zhang, H. Zhang, J. Zhang, K. Li, Y. Li, Y. Cheng, J. W. Y. Lam, W. Zhang, C.-S. Lee and B. Z. Tang, Visualizing the Initial Step of Self-Assembly and the Phase Transition by Stereogenic Amphiphiles with Aggregation-Induced Emission, *ACS Nano*, 2019, **13**, 839–846.

33 G. J. Richards, J. Labuta, J. P. Hill, T. Mori and K. Ariga, Designing Lower Critical Solution Temperature Behavior into a Discotic Small Molecule, *J. Phys. Chem. Lett.*, 2010, **1**, 1336–1340.

34 J. Zhou, W. Yuan, Y. Qing, G. Du and Q. Li, A Coordinating Small Organic Molecule with Tunable Lower Critical Solution Temperature for Efficient Management of Solar Radiation, *Macromol. Rapid Commun.*, 2024, **45**, 2400167.

35 Y. H. Chu, M. F. Cheng and Y. H. Chiang, Combinatorial discovery of small-molecule 1,2,3-triazolium ionic liquids exhibiting lower critical solution temperature phase transition, *Sci. Rep.*, 2020, **10**, 18247.

36 M. A. Martínez, D. Aranda, E. Ortí, J. Aragó and L. Sánchez, Thermodynamics of the self-assembly of N-annulated perylene bisimides in water. Disentangling the enthalpic and entropic contributions, *Org. Chem. Front.*, 2023, **10**, 1959–1967.

37 X. Li, X. Bu, J. Huang, Y. Li, L. Wang, H. Miao and G. Shi, A long-term stable thermochromic smart window of PNIPAM-based hydrogels with excellent water retention and visible light modulation, *J. Mater. Chem. A*, 2026, **14**, 10657–10667.

38 F. Jiang, K. Yu, R. Kieffer, D. D. Jong, R. M. Parker, S. Vignolini and M. E. A. Tam, Thermochromic hydrogel with high transmittance modulation and fast response for flexible smart windows, *Commun. Mater.*, 2025, **6**, 239.

39 G. Li, J. Chen, Z. Yan, S. Wang, Y. Ke, W. Luo, H. Ma, J. Guan and Y. Long, Physical crosslinked hydrogel-derived smart windows: anti-freezing and fast thermal responsive performance, *Mater. Horiz.*, 2023, **10**, 2004–2012.

40 K. Wang, S. Liu, J. Yu, P. Hong, W. Wang, W. Cai, J. Huang, X. Jiang, Y. Lai and Z. Lin, Hofmeister Effect-Enhanced, Nanoparticle-Shielded, Thermally Stable Hydrogels for Anti-UV, Fast-Response, and All-Day-Modulated Smart Windows, *Adv. Mater.*, 2025, **37**, 2418372.

41 T. Ogoshi, K. Kida and T. A. Yamagishi, Photoreversible Switching of the Lower Critical Solution Temperature in a Photoresponsive Host–Guest System of Pillar[6]arene with Triethylene Oxide Substituents and an Azobenzene Derivative, *J. Am. Chem. Soc.*, 2012, **134**, 20146–20150.

42 T. Dünnebacke, K. K. Kartha, J. M. Wiest, R. Q. Albuquerque and G. Fernández, Solvent-controlled *E*/*Z* isomerization *vs.* [2+2] photocycloaddition mediated by supramolecular polymerization, *Chem. Sci.*, 2020, **11**, 10405–10413.

43 L. B. Zou, X. L. Zhou, H. Zheng, Z. W. Fan, D. W. Pan, Z. Liu, W. Wang, R. Xie, X. J. Ju and L. Y. Chu, Regulatory effects of cyclodextrins on light-responsive phase transition behaviors of poly(*N*-isopropylacrylamide-*co*-*N*-(4-phenylazophenyl)-methylacrylamide), *Polymer*, 2024, **313**, 127676.

44 J. Cui, J. E. Kwon, H.-J. Kim, D. R. Whang and S. Y. Park, Smart Fluorescent Nanoparticles in Water Showing Temperature-Dependent Ratiometric Fluorescence Color Change, *ACS Appl. Mater. Interfaces*, 2017, **9**, 2883–2890.

45 C. Li, A. Ke, H. Shen and X. Zhang, Photonic crystal-integrated thermo-responsive smart windows with multi-color and enhanced NIR shielding, *J. Mater. Chem. A*, 2025, **13**, 18833–18841.

46 Y. Ding, Z. Wang and X. Zhang, Thermosensitive micelles formed from a small-molecule amphiphile: switchable LCST and potential application in cloud point separation, *Chem. Commun.*, 2013, **49**, 5580–5582.

47 P. P. N. Syamala and F. Würthner, Modulation of the Self-Assembly of π-Amphiphiles in Water from Enthalpy-to Entropy-Driven by Enwrapping Substituents, *Chem. – Eur. J.*, 2020, **26**, 8426–8434.

48 Y. Deng, X. Li, Q. Zhang, Z. Luo, C. Han and S. Dong, LCST phase behavior of benzo-21-crown-7 with different alkyl chains, *Beilstein J. Org. Chem.*, 2019, **15**, 437–444.

49 S. Dong, J. Heyda, J. Yuanc and C. A. Schalley, Lower critical solution temperature (LCST) phase behaviour of an ionic liquid and its control by supramolecular host–guest interactions, *Chem. Commun.*, 2016, **52**, 7970–7973.

50 P. P. N. Syamala, B. Soberats, D. Görl, S. Gekle and F. Würthner, Thermodynamic insights into the entropically driven self-assembly of amphiphilic dyes in water, *Chem. Sci.*, 2019, **10**, 9358–9366.

51 S. Wu, H. Sun, M. Duan, H. Mao, Y. Wu and H. Zhao, Applications of thermochromic and electrochromic smart windows: Materials to buildings, *Cell Reports Phys. Sci.*, 2023, **4**, 101370.

52 D. Wang, G. Chen and J. Fu, Multifunctional thermochromic smart windows for building energy saving, *J. Mater. Chem. A*, 2024, **12**, 12960–12982.

53 K. Lei, Q. Jiang, D. Gong, W. Wang, J. Wu, Q. Chang, G. Wang and X. Pang, Hydrogel Smart Windows: Working Mechanisms, Recent Developments, and Perspectives, *Small*, 2025, **21**, e10382.

54 P. Wei, J.-X. Zhang, Z. Zhao, Y. Chen, X. He, M. Chen, J. Gong, H. H. Y. Sung, I. D. Williams, J. W. Y. Lam and B. Z. Tang, Multiple yet Controllable Photoswitching in a Single AIEgen System, *J. Am. Chem. Soc.*, 2018, **140**, 1966–1975.

55 Y. Shao, W. Li, M. Cametti, Z. Džolić, Z. Ding, Z. Yang, Y. Xie and S. Jiang, Single-Component High-Performance

Adhesives Enabled by Synergistic Supramolecular and Covalent Polymerization, *J. Am. Chem. Soc.*, 2025, **147**, 23868–23877.

56 N. F. König, D. Mutruc and S. Hecht, Accelerated Discovery of α-Cyanodiarylethene Photoswitches, *J. Am. Chem. Soc.*, 2021, **143**, 9162–9168.

57 D. Görl, B. Soberats, S. Herbst, V. Stepanenko and F. Würthner, Perylene bisimide hydrogels and lyotropic liquid crystals with temperature-responsive color change, *Chem. Sci.*, 2016, **7**, 6786–6790.

58 R. Colaco, C. Appiah and A. Staubitz, Controlling the LCST-Phase Transition in Azobenzene-Functionalized Poly(*N*-Isopropylacrlyamide) Hydrogels by Light, *Gels*, 2023, **9**, 75.

59 R. Colaco, N. Wolf, P. Hepke, R. Renken and A. Staubitz, Superswelling, Supershrinking, and a Broadened Phase Transition—Amphiphilic Thermosensitivity in Sulfonate-Functionalized Azobenzene-*co*-NIPAAm Hydrogels and Polymers, *ACS Appl. Polym. Mater.*, 2025, **7**, 13896–13906.